

NASA TECHNICAL MEMORANDUM

NASA TM X-73371

THE ROLE OF FRACTURE MECHANICS IN THE DESIGN OF FUEL TANKS IN SPACE VEHICLES

(NASA-TM-X-73371) THE ROLE OF FRACTURE
MECHANICS IN THE DESIGN OF FUEL TANKS IN
SPACE VEHICLES (NASA) SC F EC 203/NE 001

B77-22168

CSCI 222

Unclass
25126

G3/18

By Stephen J. Denton and C. K. Liu
Program Development

December 1976

NASA



*George C. Marshall Space Flight Center
Marshall Space Flight Center, Alabama*

TECHNICAL REPORT STANDARD TITLE PAGE

1. REPORT NO. NASA TM X-73371	2. GOVERNMENT ACCESSION NO.	3. RECIPIENT'S CATALOG NO.	
4. TITLE AND SUBTITLE The Role of Fracture Mechanics in the Design of Fuel Tanks in Space Vehicles		5. REPORT DATE December 1976	6. PERFORMING ORGANIZATION CODE
		8. PERFORMING ORGANIZATION REPORT #	
7. AUTHOR(S) Stephen J. Denton and C. K. Liu*		10. WORK UNIT NO.	11. CONTRACT OR GRANT NO.
9. PERFORMING ORGANIZATION NAME AND ADDRESS George C. Marshall Space Flight Center Marshall Space Flight Center, Alabama 35812		13. TYPE OF REPORT AND PERIOD COVERED Technical Memorandum	
		14. SPONSORING AGENCY CODE	
12. SPONSORING AGENCY NAME AND ADDRESS National Aeronautics and Space Administration Washington, D. C. 20546		15. SUPPLEMENTARY NOTES Prepared by Preliminary Design Office, Program Development *Dr. Liu is a Professor of Mechanical Engineering at the University of Alabama, University, Alabama. A member of the 1976 NASA-ASEE Summer Faculty Fellowship Program, he will continue this study during the second year of this fellowship.	
16. ABSTRACT <p>With special reference to design of fuel tanks in space vehicles, the principles of fracture mechanics are reviewed. An approximate but extremely simple relationship among (1) the operating stress level, (2) the length of crack, and (3) the number of cycles of failure is derived, from which any one of the variables can be computed approximately from the knowledge of the other two, if the loading schedule (mission of the tank) is not greatly altered.</p> <p>Two sample examples illustrating the procedures of determining the allowable safe operating stress corresponding to a set of assumed loading schedule is included in this report. The selection of sample examples is limited by the relatively meager available data on the candidate material for various stress ratios in the cycling.</p>			
17. KEY WORDS		18. DISTRIBUTION STATEMENT Unclassified - Unlimited	
19. SECURITY CLASSIF. (of this report) Unclassified	20. SECURITY CLASSIF. (of this page) Unclassified	21. NO. OF PAGES 50	22. PRICE NTIS

TABLE OF CONTENTS

	Page
SUMMARY	1
INTRODUCTION	1
FUNDAMENTALS OF CRACK ANALYSIS	2
CRACK-TIP STRESS FIELDS FOR ISOTROPIC ELASTIC BODIES	5
CRACK GROWTH	16
ILLUSTRATIVE EXAMPLES	21
Example I	21
Example II	30
EQUATION (15) AND ITS MEANING	36
DISCUSSIONS	37
CONCLUSIONS	41
REFERENCES	43

LIST OF ILLUSTRATIONS

Figure	Title	Page
1.	Stress and displacement fields near the leading edge of a crack	6
2.	An infinite cracked sheet with uniform normal stress at infinity	7
3.	A crack in an infinite sheet subjected to centrally applied wedge forces	8
4.	An edge crack in a semiinfinite sheet subjected to tension	9
5.	A single edge cracked strip subjected to tension	10
6.	Double-symmetric edge cracks in a strip of finite length subjected to tension	12
7.	An edge crack in a strip subjected to in-plane bending	13
8.	Penny-shaped crack (circular disk) in an infinite solid subjected to uniform tension	14
9.	An elliptical crack in an infinite solid subjected to uniform tension	15
10.	Correlation of data on 2024-T3 aluminum alloy	17
11.	Product of stress intensity and number of cycles as a function of aft crack length	19
12.	Relationship between the stress intensity and number of cycles for constant value of crack length	20
13.	An approximate relationship among σ/Λ , ΔN , and a [equation (15)]	22

LIST OF ILLUSTRATIONS (Concluded)

Figure	Title	Page
14.	Operating stress levels in a 2219-T87 aluminum tank for a given loading schedule	26
15.	History of cyclic stresses in 2219-T87 aluminum tank . . .	28
16.	Operating stress levels in a 6 Al-4V titanium tank for a given loading schedule	32
17.	History of cyclic stresses in 6 Al-2.5 Sn titanium tank . . .	33
18.	σ versus ΔN 5 Al-2.5 Sn titanium tank for a specific loading schedule	38

LIST OF TABLES

Table	Title	Page
1.	Single Edge Cracked Strip Subjected to Tension	11
2.	Double-Symmetric Edge Cracks in a Strip of Finite Length Subjected to Tension	12
3.	Edge Crack in a Strip Subjected to In-Plane Bending	13
4.	Typical Threshold Stress-Intensity Data for Various Material/ Environment Combinations	24

TECHNICAL MEMORANDUM X-73371

THE ROLE OF FRACTURE MECHANICS IN THE DESIGN OF FUEL TANKS IN SPACE VEHICLES

SUMMARY

As air and spacecraft have progressed to higher and higher performance, the materials of construction have had to answer to greater demands placed upon them — increased strength and increased durability. The unfortunate alternative is the occurrence of sudden catastrophic structural failure. The metal industry has responded to this challenge by developing new, higher strength sheets, aluminum and other alloys, and by finding ways to glean increased strength from existing materials. As nature has it, however, one does not get something for nothing. When drawing more of one characteristic out of a material, one must be prepared to accept a lesser measure of other, also desirable, characteristics. Therefore, it has happened that the increases in tensile strength of metals and alloys have been paid for in toughness, ductility, and propensity for brittle failure where experience with lesser strength materials would indicate ductile failure or no failure at all.

The development of stronger structural materials, of wider variety, increases the problem of safe design and proper selection. The consequence of an inadequate solution to these problems is obvious, namely, unlimited crack propagation at nominal stresses well below the strength capability of the material. To eliminate or lessen these catastrophic consequences, one seeks an understanding of the fracture behavior of various materials systems to complement selection and design practice.

INTRODUCTION

Proposed concepts of future advanced launch vehicle systems involve structures which characteristically are of unprecedented large size, require high structural efficiency, and must meet long service life because of the

economic consideration of reusability. In keeping with the original objective of this research task, which was to improve current capabilities of evaluating structural weights and characteristics of proposed structural designs for this class of vehicle, this task was oriented specifically to the development of a simplified analytical procedure to assess fracture mechanics design requirements suitable for use in conceptual and preliminary design studies.

Metallic materials generally have the characteristics of reduced fracture toughness and ductility, resulting in greater tendency to brittle failure, when the basic material strength is increased either through alloying or heat treatment. This fact, coupled with the standard conceptual and preliminary design practice of basing analytical weight estimates on strength requirements with a factor of safety, can lead to misleading and erroneous results. This is particularly the case for the vehicle class under study because of its extreme service life requirements and weight sensitivity. Sometimes, in an attempt to compensate for this shortcoming, a higher than normal factor of safety for strength calculations is used or a large weight contingency is added. This approach, however, produces almost arbitrary results and provides no data for candidate material selection.

In a conceptual design study phase where many alternate structural configurations and design concepts are being evaluated, it is impractical to conduct a rigorous fracture mechanics analysis of each case because of the time involved and the general lack of definitive design data. Consequently, this research task attempts to develop, in an approximate sense, an analytical procedure which will provide a quantitative assessment of the fracture design requirements and is suitable for conceptual and preliminary design usage.

FUNDAMENTALS OF CRACK ANALYSIS

In his pioneering paper on equilibrium and stability of cracks, Griffith [1] viewed the change in potential energy in a body into which a crack is introduced. His analysis is complete and correct when applied to "perfectly brittle" materials, such as glass.

Consider an infinite sheet of elastic material subject to uniform biaxial stress, σ , at infinity into which a through crack of length $2a$ is subsequently introduced. Let U denote the potential energy of the system, where U_0 is the

potential energy prior to introducing the crack. Upon introducing the crack, U may be written

$$U = U_o - U_a + U_T \quad (1)$$

where U_a is the decrease in the potential energy of deformation (strain energy and boundary face work) and U_T is the increase in surface energy due to the new surface. From the work of Inglis [2],

$$U_a = \frac{\pi\sigma^2 a^2 t}{E} \quad (2)$$

where t is the thickness of the sheet and E is the modulus of elasticity of the material. The surface energy term U_T , being the product of the surface tension of the material and the new crack surface, is written as

$$U_T = 4atT \quad (3)$$

Substitution of equations (2) and (3) into equation (1) yields

$$U = U_o - \frac{\pi\sigma^2 a^2 t}{E} + 4atT \quad (4)$$

To ascertain the equilibrium crack size, the first variation of the potential energy should be set to zero; hence,

$$\delta U = \left(-\frac{2\pi\sigma^2 at}{E} + 4tT \right) \delta a = 0 \quad (5)$$

or

$$\sigma\sqrt{a} = \sqrt{\frac{2ET}{\pi}} \quad (6)$$

Equation (6) is the equilibrium condition for a crack in a perfectly brittle material.

On further differentiating of equation (5), one always obtains for the second variation of the potential energy U,

$$\delta^2 U = \left(-\frac{2\pi\sigma^2 t}{E} \right) \delta a^2 < 0 \quad (7)$$

The negativeness of $\delta^2 U$ in equation (7) indicates that equation (6) describes an unstable-equilibrium condition corresponding to a maximum potential energy

$$U_{\max} = U_0 + 2atT$$

Experimentally, Griffith verified his theory by obtaining the values for the right-hand side of equation (6) as

$$\sqrt{\frac{2ET}{\pi}} = 137 \frac{\text{lb}}{\text{in.}^2} \sqrt{\text{in.}}$$

He confirmed this conclusion by having a good agreement on tubes and spheres of glass with prepared cracks. He stated

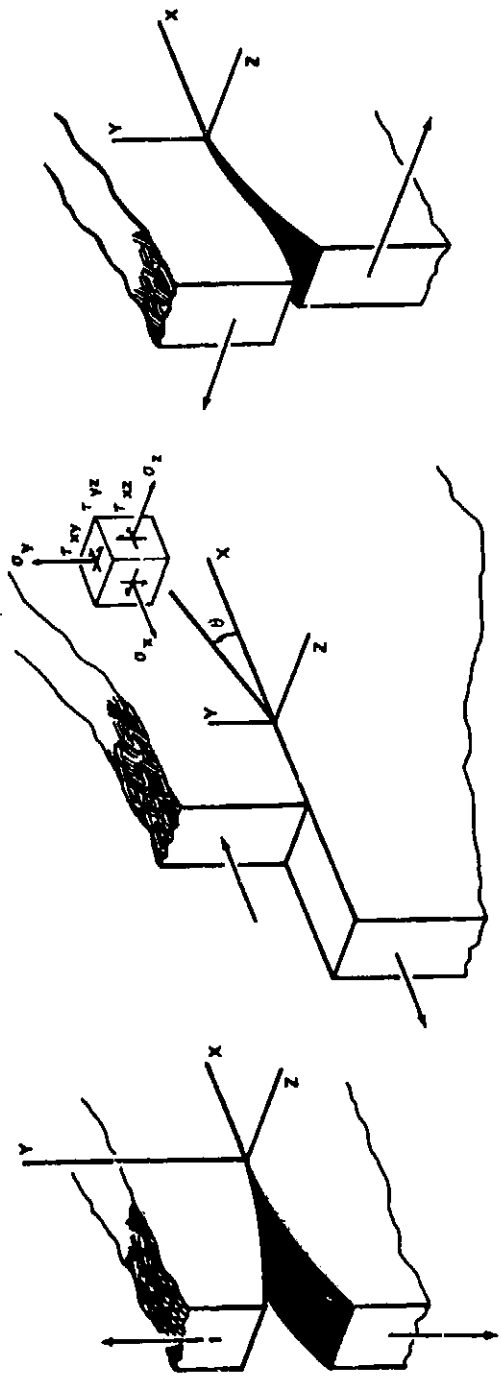
$$\sigma\sqrt{a} = \text{Constant (for glass at least)}$$

It is interesting to note that this conclusion is reached also from much more recent experiments on crack growth rate data and to note, too, that this constant is not an absolute constant, but is dependent on the number of loading cycles, operating stress level, and other characteristics of the material under consideration. This will be discussed in a later section after the terms crack-tip stress intensity factor K_I and K_{IC} are introduced.

CRACK-TIP STRESS FIELDS FOR ISOTROPIC ELASTIC BODIES

The stress fields near crack tips can be divided into three basic types, each associated with a local mode of deformation as illustrated in Figure 1. The opening, Mode I, is associated with local displacements in which the crack surfaces move directly apart, being symmetric with respect to the X-Y and X-Z planes. The edge-slidings, Mode II, is characterized by displacements in which the crack surfaces slide over one another perpendicularly to the leading edge of the crack, being symmetric with respect to the X-Y plane and skew-symmetric with respect to the X-Z plane. Tearing, Mode III, has the crack surfaces sliding with respect to one another parallel to the leading edge, being skew-symmetric with respect to the X-Y and X-Z planes. A general case of crack-tip deformation and stress fields can be realized by superposition of these three modes. The resulting stress and displacement fields are appended in the figure under their respective mode descriptions.

The coefficients in the expressions for the stresses and displacements for all three modes contain three parameters -- K_I , K_{II} , and K_{III} . These are crack-tip stress-intensity factors which are not dependent on the coordinates r and θ ; hence, they control the intensity of the stress field, but not its distribution. It can be seen that these factors must contain the magnitude of loading forces linearly for linear elastic bodies and must also depend on the configuration of the body including the crack size. Consequently, it seems logical to suggest that unstable crack extension will take place when the intensity, K_I , reaches a critical value, K_{IC} , where K_{IC} is a material property (i. e., the material's ability to withstand a given intensity of crack-tip stress field, K_I).



MODE I:

$$\sigma_z = \frac{K_I}{(2\pi r)^{1/2}} \cos \frac{\theta}{2} \left[1 - \sin \frac{\theta}{2} \sin \frac{3\theta}{2} \right]$$

$$\sigma_x = \frac{K_I}{(2\pi r)^{1/2}} \cos \frac{\theta}{2} \left[1 + \sin \frac{\theta}{2} \sin \frac{3\theta}{2} \right]$$

$$\tau_{xy} = \frac{K_I}{(2\pi r)^{1/2}} \sin \frac{\theta}{2} \cos \frac{3\theta}{2}$$

$$\sigma_z = \nu(\sigma_x - \sigma_y), \quad \tau_{yz} = \tau_{xz} = 0$$

$$u = \frac{K_I}{G} \left[r/(2\pi) \right]^{1/2} \cos \frac{\theta}{2} \left[1 - 2\nu + \sin^2 \frac{\theta}{2} \right]$$

$$v = \frac{K_I}{G} \left[r/(2\pi) \right]^{1/2} \sin \frac{\theta}{2} \left[2 - 2\nu - \cos^2 \frac{\theta}{2} \right]$$

$$w = 0$$

MODE II:

$$\sigma_z = \frac{K_{II}}{(2\pi r)^{1/2}} \sin \frac{\theta}{2} \left[2 + \cos \frac{\theta}{2} \cos \frac{3\theta}{2} \right]$$

$$\sigma_y = \frac{K_{II}}{(2\pi r)^{1/2}} \sin \frac{\theta}{2} \cos \frac{3\theta}{2}$$

$$\tau_{xy} = \frac{K_{II}}{(2\pi r)^{1/2}} \cos \frac{\theta}{2} \left[1 - \sin \frac{\theta}{2} \sin \frac{3\theta}{2} \right]$$

$$\sigma_z = \nu(\sigma_x + \sigma_y), \quad \tau_{xz} = \tau_{yz} = 0$$

$$u = \frac{K_{II}}{G} \left[r/(2\pi) \right]^{1/2} \sin \frac{\theta}{2} \left[2 - 2\nu + \cos^2 \frac{\theta}{2} \right]$$

$$v = \frac{K_{II}}{G} \left[r/(2\pi) \right]^{1/2} \cos \frac{\theta}{2} \left[-1 + 2\nu + \sin^2 \frac{\theta}{2} \right]$$

$$w = 0$$

MODE III:

$$\tau_{xy} = -\frac{K_{III}}{(2\pi r)^{1/2}} \sin \frac{\theta}{2}$$

$$\tau_{yz} = \frac{K_{III}}{(2\pi r)^{1/2}} \cos \frac{\theta}{2}$$

$$\sigma_x = \sigma_y = \sigma_z = \tau_{xz} = 0$$

$$w = \frac{K_{III}}{G} \left[(2r/\pi) \right]^{1/2} \sin \frac{\theta}{2}$$

$$u = v = 0$$

Figure 1. Stress and displacement fields near the leading edge of a crack (coordinates as shown).

Two important and contrasting cases are worth mentioning:

1. Case I — An infinite plate subjected at infinity to uniform tensile stress in which a transverse crack of length $2a$ is introduced. In this important case, it can be shown (Fig. 2) that

$$K_I = \sigma \sqrt{\pi a}$$

$$K_{II} = 0$$

$$K_{III} = 0$$

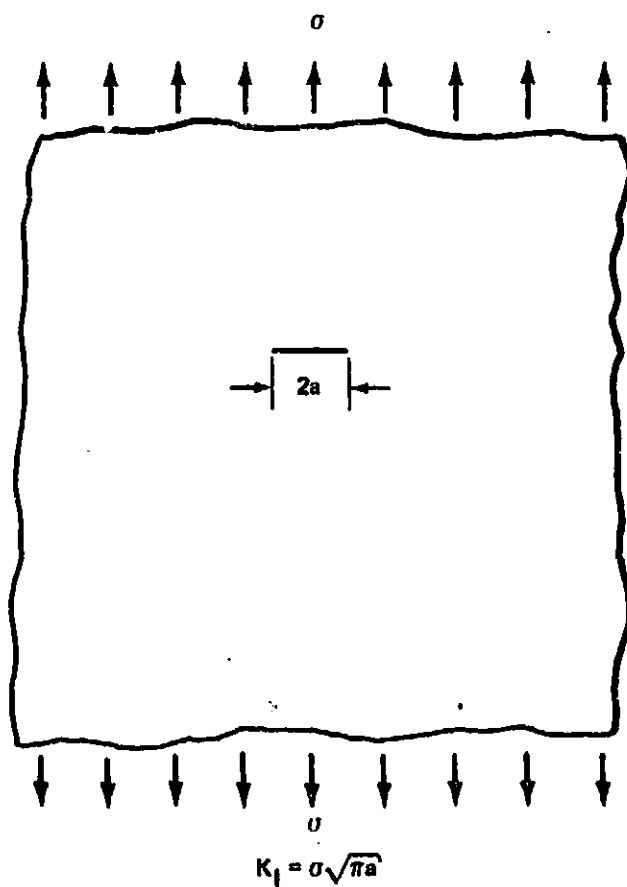


Figure 2. An infinite cracked sheet with uniform normal stress at infinity.

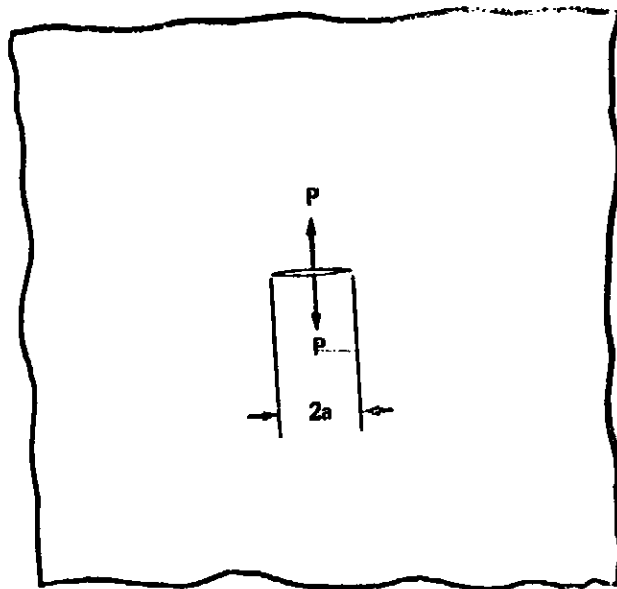
It is significant to note that, had the sheet been finite, the intensity factor would be, as suggested by Irwin [3],

$$K_I = \sigma \sqrt{W \tan \frac{\pi a}{W}} ,$$

where W is the finite width of the strip or plate.

2. Case II — A crack centrally located in an infinite sheet subjected to a pair of equal and opposite wedge forces, P , is introduced. In this case, it can be shown (Fig. 3) that

$$K_I = \frac{P}{\sqrt{\pi a}} .$$



$$K_I = \frac{P}{\sqrt{\pi a}}$$

Figure 3. A crack in an infinite sheet subjected to centrally applied wedge forces.

It will be observed that, in this case, the stress-intensity factor decreases with increasing crack length, quite a contrast to the previously mentioned case.

Other interesting cases are:

1. Case III — An edge crack in a semiinfinite sheet subjected to tension (Fig. 4).

$$K_I = 1.12 \sigma \sqrt{\pi a}$$

It is seen that the free surface correction factor is 1.12 for edge notches.

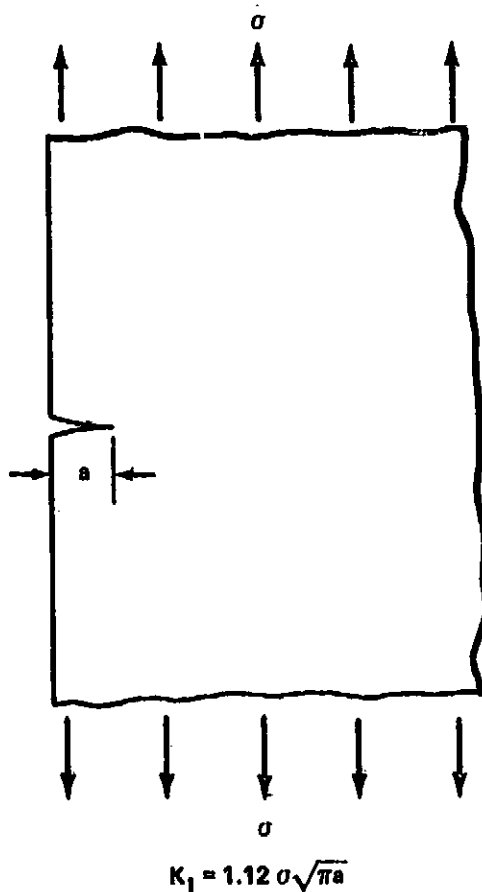


Figure 4. An edge crack in a semiinfinite sheet subjected to tension.

2. Case IV — A single edge-cracked strip subjected to tension (Fig. 5).

$$K_I = \sigma \sqrt{\pi a} k \left(\frac{2a}{W} \right)$$

where $k(2a/W)$ is given as a function of $2a/W$ in Table 1.

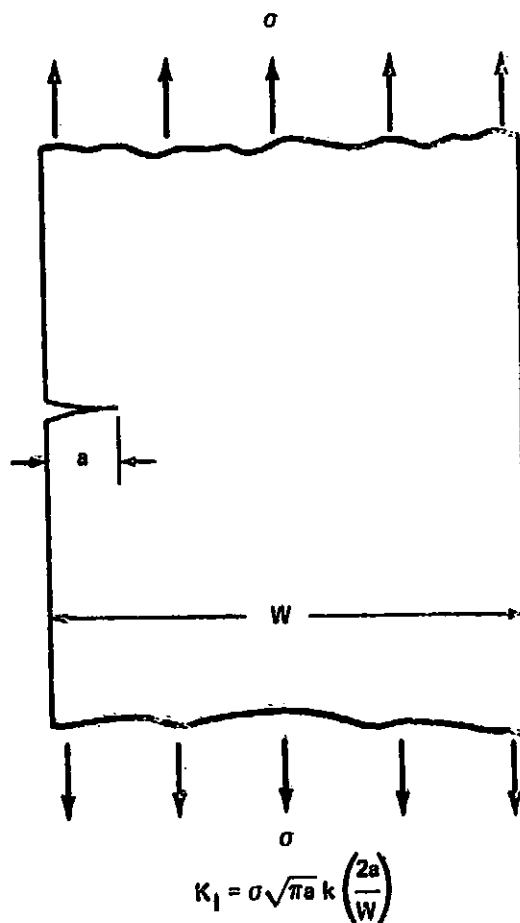


Figure 5. A single edge cracked strip subjected to tension.

TABLE 1. SINGLE EDGE CRACKED STRIP
SUBJECTED TO TENSION

2a/W	k(2a/W)
0.1	1.14
0.2	1.19
0.3	1.29
0.4	1.37
0.5	1.50
0.6	1.66
0.7	1.87
0.8	2.12
0.9	2.44
1.0	2.82

3. Case V — Double-symmetric edge cracks in a strip of finite length subjected to tension (Fig. 6).

$$K_I = \sigma \sqrt{\pi a} \left(\frac{W}{\pi a} \tan \frac{\pi a}{W} \right)^{1/2} h \left(\frac{2a}{W} \right) ,$$

where $h(2a/W)$ is given in Table 2 for various values of $2a/W$.

4. Case VI — An edge crack in a strip subjected to in-plane bending (Fig. 7).

$$K_I = \frac{6M}{(H-a)^{3/2}} g(a/H) ,$$

where $g(a/H)$ is given in Table 3.

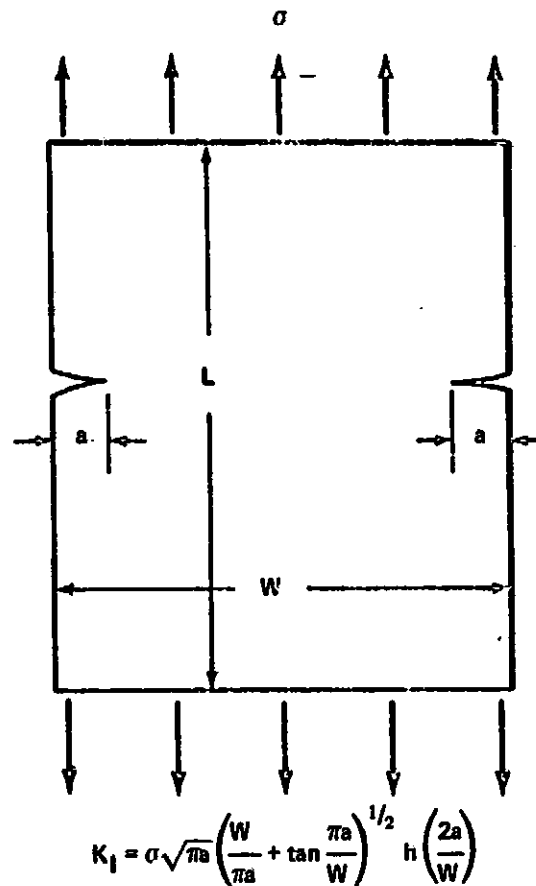
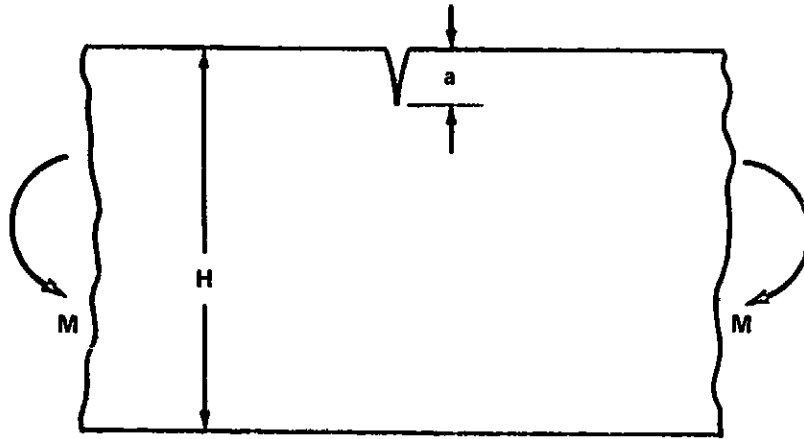


Figure 6. Double-symmetric edge cracks in a strip of finite length subjected to tension.

TABLE 2. DOUBLE-SYMMETRIC EDGE CRACKS IN A STRIP OF FINITE LENGTH SUBJECTED TO TENSION

2a/W	h(2a/W)		
	2L/W = 1	2L/W = 3.00	2L/W
0.1	1.13	1.12	1.12
0.2	1.13	1.11	1.12
0.3	1.14	1.09	1.13
0.4	1.16	1.06	1.14
0.5	1.14	1.02	1.15
0.6	1.10	1.01	1.22
0.7	1.02	1.00	1.34
0.8	1.01	1.00	1.57
0.9	1.00	1.00	2.09



$$K_I = \frac{6M}{(H-a)^{3/2}} g(a/H)$$

Figure 7. An edge crack in a strip subjected to in-plane bending.

TABLE 3. EDGE CRACK IN A STRIP SUBJECTED TO IN-PLANE BENDING

a/H	g(a/H)
0.05	0.36
0.1	0.49
0.2	0.60
0.3	0.66
0.4	0.69
0.5	0.72
0.6	0.73
(and larger)	

5. Case VII — Penny-shaped crack in an infinite solid subjected to uniform tension [4] (Fig. 8).

$$K_I = 2\sigma \sqrt{\frac{a}{\pi}}$$

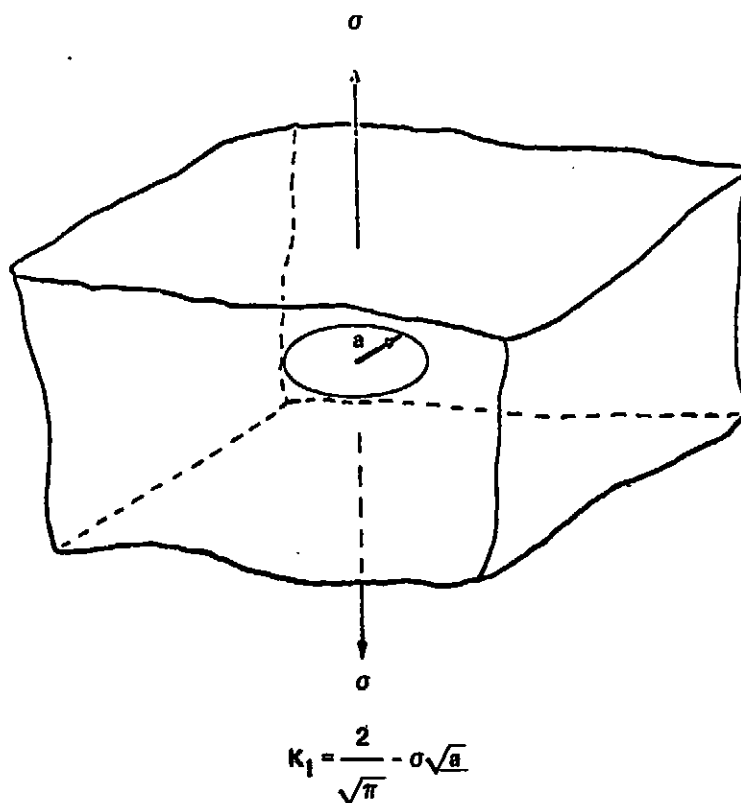


Figure 8. Penny-shaped crack (circular disk) in an infinite solid subjected to uniform tension.

6. Case VIII — Elliptical crack in an infinite solid subjected to uniform tension [5] (Fig. 9).

$$K_I = \frac{\sigma}{Q} \sqrt{\pi a} \left(\sin^2 \beta + \frac{a^2}{b^2} \cos^2 \beta \right)^{1/4}$$

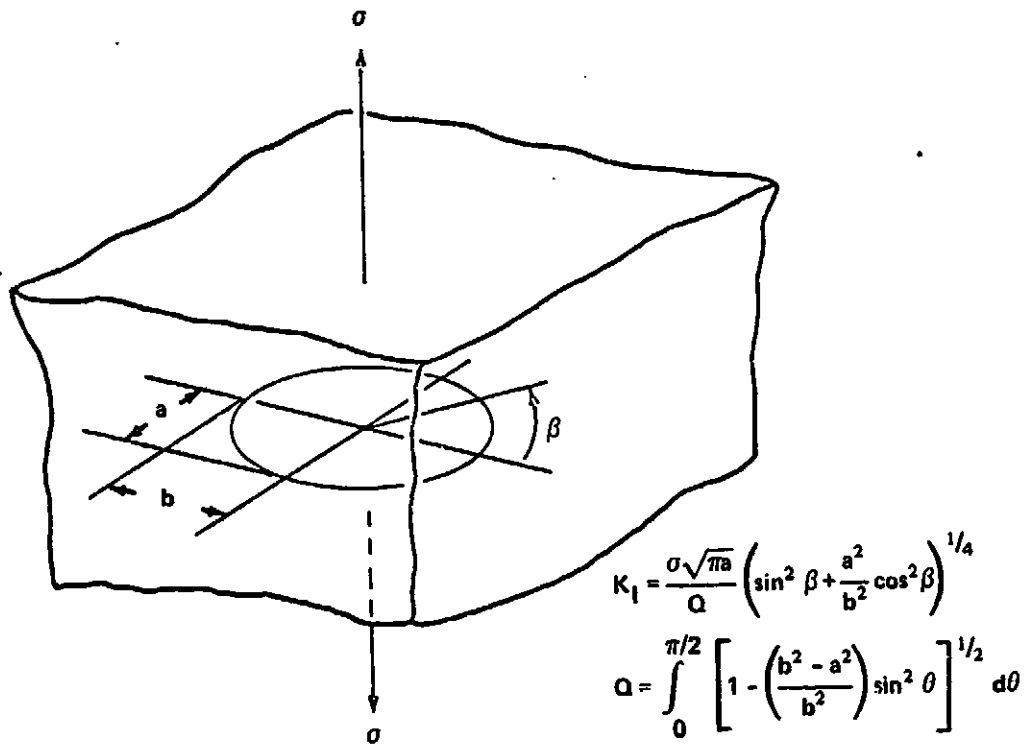


Figure 9. An elliptical crack in an infinite solid subjected to uniform tension.

where

$$Q = \int_0^{\pi/2} \left[1 - \left(\frac{b^2 - a^2}{b^2} \right) \sin^2 \theta \right]^{1/2} d\theta$$

Note that when $b \rightarrow \infty$ and $\beta = \pi/2$,

$$K_I = \sigma \sqrt{\pi a} \quad (\text{Case I}) \quad ;$$

when $b = a$,

$$K_I = 2\sigma \sqrt{\frac{a}{\pi}} \quad (\text{Case VII}) \quad .$$

CRACK GROWTH

In a multitude of applications of engineering structures, the loading is likely a fluctuating one. One eminent example is the proof testing of structural components of space vehicles, such as the tanks, nozzles, etc. Clearly, the component is subjected to repeated application of the load prior to actual operation. Consequently, the useful life of the structure or component in question is often governed by "fatigue."

It has been observed that cracks existing in structures subjected to fluctuating loads grow a certain amount during each cycle of loading. As an approximation, it is assumed that the crack growth is a continuous process; that is, the growth (Δa) in a small number of cycles (ΔN) may be considered to be related to the slope of a continuous crack length a versus cycle number N curve; namely,

$$\frac{\Delta a}{\Delta N} \sim \lim_{\Delta N \rightarrow 0} \frac{\Delta a}{\Delta N} = \frac{da}{dN} \quad . \quad (8)$$

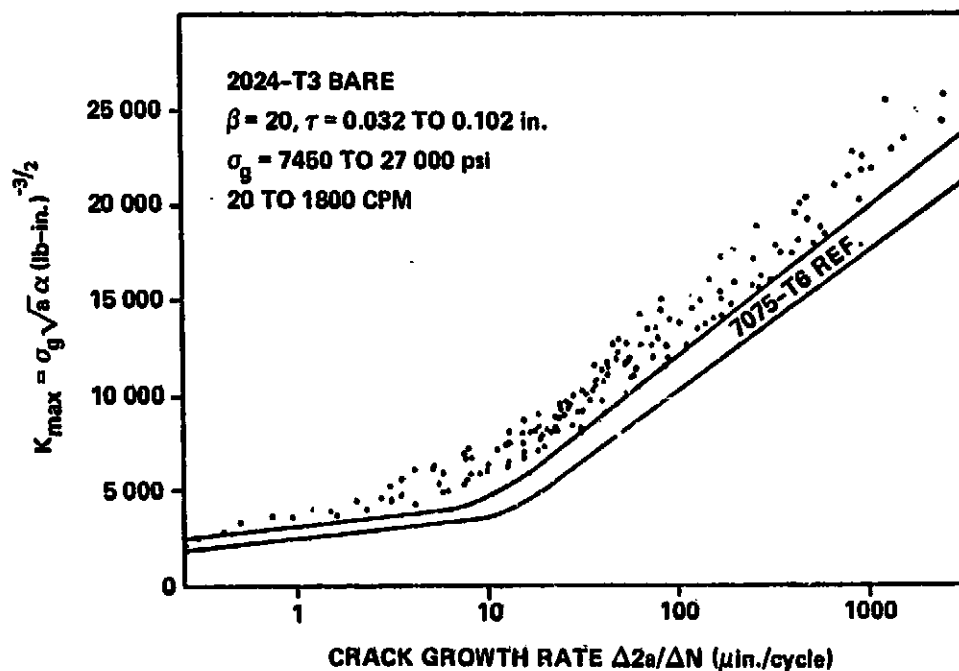
It is conceivable that this quantity is a function of (1) the material, (2) structural configuration, including the crack, (3) the environment (temperature, corrosive agents, etc.), and (4) the load-time history. Hence,

$$\frac{da}{dN} = f(K, t, N, \text{ etc.}) \quad . \quad (9)$$

But Paris [6] has hypothesized, with collaborating evidence, that "the rate of growth of a fatigue crack in a given material and environment depends, uniquely, on the local time-history of the stress-intensity factor, K ."

A typical plot of K_{\max} versus $\Delta(2a)/\Delta N$ for bare 2024-T3 aluminum alloy from three sources is shown in Figure 10, where σ is the stress-intensity factor and α is the correction factor for finite panel width, W .

$$\alpha = \sqrt{\frac{W}{\pi a} \tan \frac{\pi a}{W}} \quad (10)$$



NOTE: TESTS FROM BAC AND NACA TN 4394 AND PROCEEDINGS, THIRD CONGRESS OF APPLIED MECHANICS, 1958, pp. 595-604.

Figure 10. Correlation of data on 2024-T3 aluminum alloy.

Thus, from equation (9),

$$\frac{d(2a)}{dN} = f \left(\sigma \sqrt{a} \sqrt{\frac{W}{\pi a} \tan \frac{\pi a}{W}} \right) \quad (11)$$

From the semilogarithmic plot of data, the right-hand side of equation (11) can be approximated by the argument multiplied by a constant. It follows then

$$\frac{d(2a)}{dN} = \frac{\sigma}{A} \sqrt{a} \sqrt{\frac{W}{\pi a} \tan \frac{\pi a}{W}} \quad (12)$$

where A is a constant, having a unit of stress intensity. Equation (12) can be integrated analytically at once. The result is

$$\begin{aligned} \frac{\sigma}{a\sqrt{W}} \Delta N = \frac{1}{\sqrt{2\pi}} \ln \left(\frac{\tan \frac{\pi a}{W} + \sqrt{2} \tan^{1/2} \frac{\pi a}{W} + 1}{\tan \frac{\pi a}{W} - \sqrt{2} \tan^{1/2} \frac{\pi a}{W} + 1} \right) \\ + \frac{2}{\sqrt{2\pi}} \arctan \frac{\sqrt{2} \tan^{1/2} \frac{\pi a}{W}}{1 - \tan \frac{\pi a}{W}} \quad (13) \end{aligned}$$

Equation (13) is depicted graphically in Figure 11. Figure 12 shows another plot of equation (13) where the crack length is treated as a parameter.

It is seen that the curve in Figure 11 can be closely approximated, especially at low values of crack lengths, by the simple relation

$$\frac{\sqrt{\pi}}{4} \frac{\sigma}{A\sqrt{W}} \Delta N = \sqrt{\frac{\pi a}{W}} \quad (14)$$

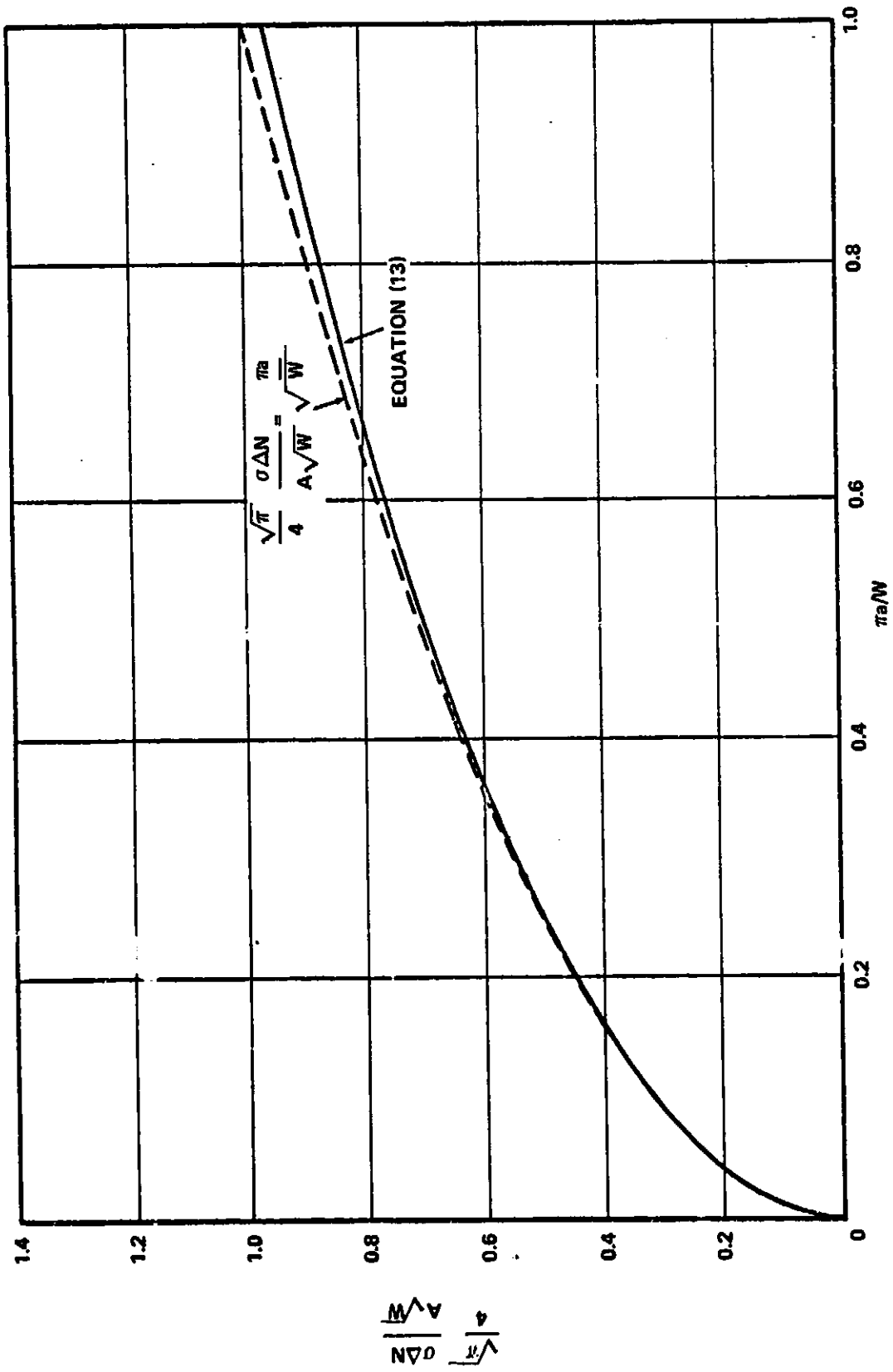


Figure 11. Product of stress intensity and number of cycles as a function of aft crack length.

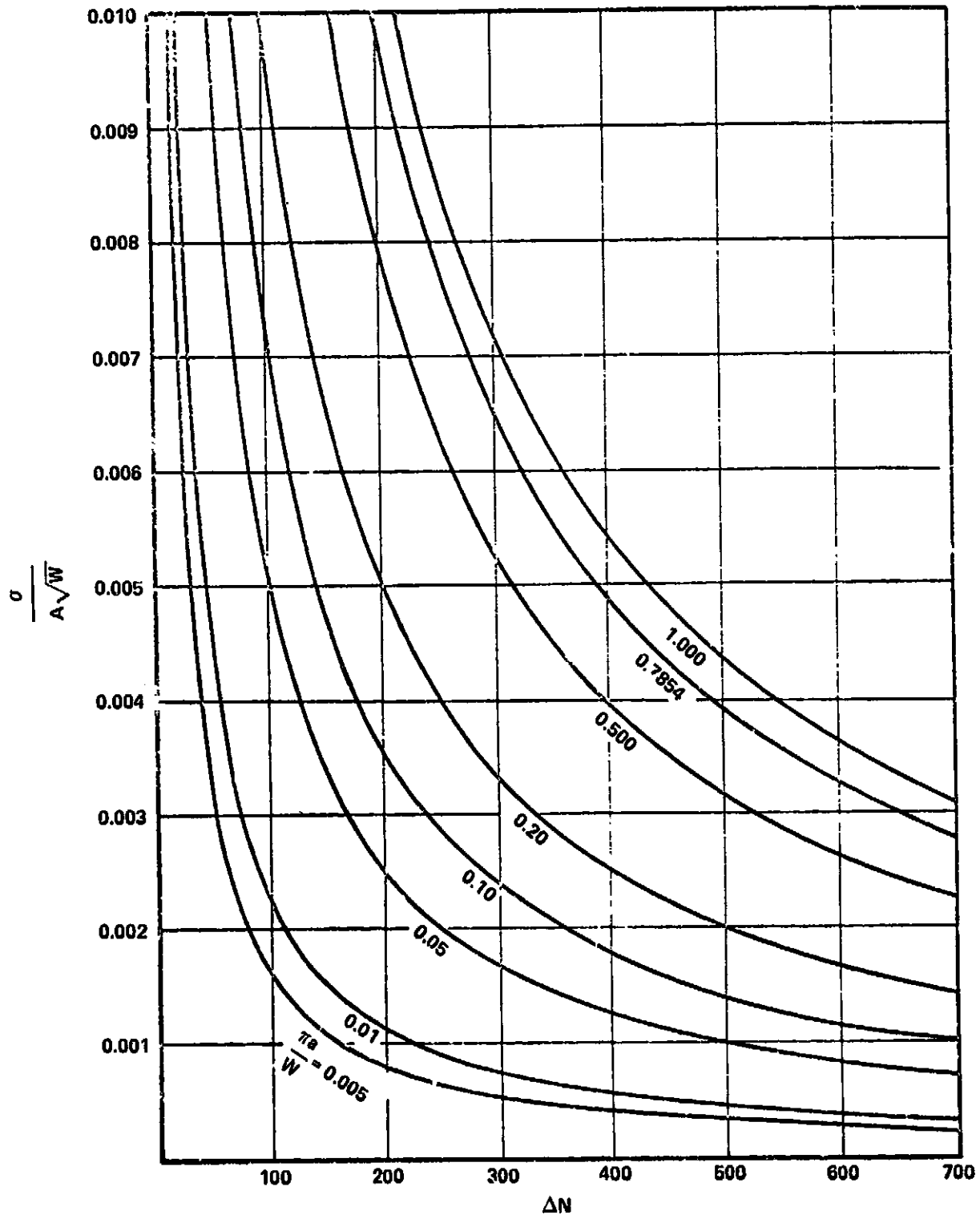


Figure 12. Relationship between the stress intensity and number of cycles for constant value of crack length.

With this approximate formulation, it is possible to correlate among three significant parameters (σ , N , and a) with a greatly simplified equation:

$$\frac{\sigma}{A} \frac{\Delta N}{\sqrt{a}} = 2 \quad (15)$$

If the constant A is identified for a specific material and a certain prescribed loading condition, the value of any one of the parameters can be immediately estimated by knowing the other two. A plot of σ/A versus ΔN is given in Figure 13 for several values of a .

ILLUSTRATIVE EXAMPLES

To delineate the design procedures according to the principles of fracture mechanics previously mentioned, it will be advisable (and economical) to "paper design" a pressure tank under several sets of hypothetical loading conditions and requirements. These requirements and loading conditions (or schedules) are as follows:

Example I

1. Material:
 - a. 2219-T87 aluminum
 - b. Operating temperature, -423°F
 - c. Fluid environment, helium
 - d. Yield stress, $\sigma_{ys} = 70.5 \text{ ksi}$
 - e. Ultimate stress, 87 ksi
 - f. Critical stress intensity factor, $K_{IC} = 32.8 \text{ ksi}$

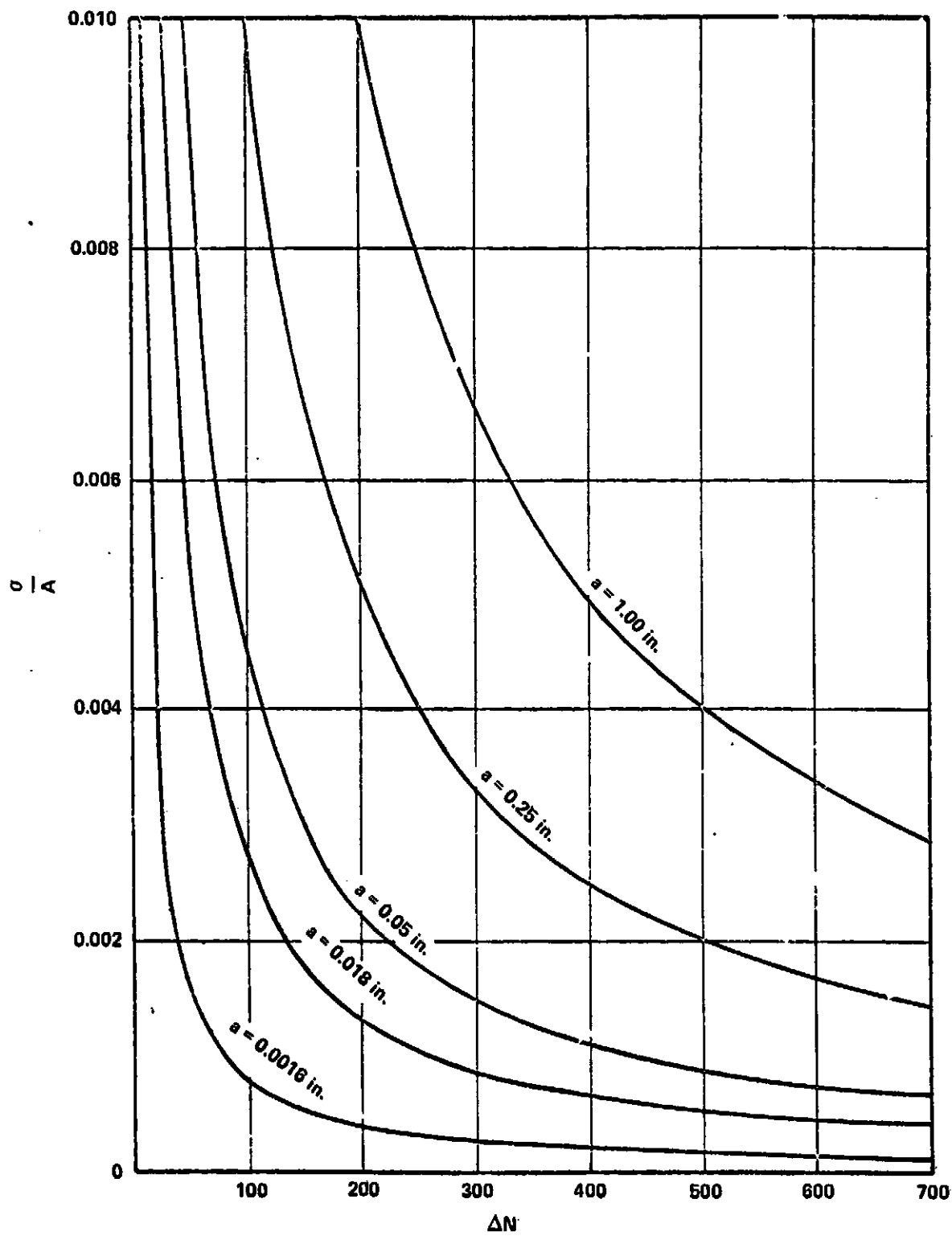


Figure 13. An approximate relationship among σ/Λ , ΔN , and a [equation (15)].

2. Loading schedules:

a. 300 cycles in which the pressure (or stress) changes from 50 to 100 to 50 percent of the maximum operating pressure (or stress); i. e.,

$$R = \frac{\text{minimum stress}}{\text{maximum stress}} = 0.5$$

b. 150 cycles in which the pressure (or stress) changes from 0 to 90 to 0 percent of the maximum operating pressure (or stress); i. e., $R = 0.0$.

c. 50 cycles in which the pressure (or stress) changes from 0 to 95 to 0 percent of the maximum operating pressure (or stress); i. e., $R = 0.0$.

d. 8 days at 100 percent of maximum operating pressure (or stress σ_{op}).

3. Tank outside diameter 400 in.; maximum operating pressure 40 psig.

In view of the fact that pressure tanks must not allow any surface cracks to develop to any depth comparable to the thickness of the tank, the designer regards the tank as a thick-walled tank, as opposed to a thin-walled tank.

Further, it has been observed that there exists a threshold stress-intensity level for a given material in a given environment. That is to say that below a given value of stress intensity, or K_{II}/K_{IC} ratio, crack growth has not been detected; above this value, crack growth does occur and can result in fracture. This stress intensity is known as the threshold stress intensity K_{TH} , likewise, K_{TH}/K_{IC} , the threshold stress intensity ratio. Table 4 lists typical threshold stress-intensity ratios for various materials under various environmental conditions.

With respect to the case under consideration, namely 2219-T87 aluminum plate with helium environment, this apparent threshold stress-intensity ratio should be 0.90 (>0.85). Moreover, the curves of K_{II}/K_{IC} versus cycles to failure for 2219-T87 aluminum under two loading conditions (i. e., $R = 0.0$ and $R = 0.5$) are given in Figure 14.

TABLE 4. TYPICAL THRESHOLD STRESS-INTENSITY DATA FOR VARIOUS MATERIAL/ ENVIRONMENT COMBINATIONS

Material	Temperature ^a (°F)	σ_{ys}^b (ksi) ^c	Fluid Environment	$\frac{K_{TH}}{K_{IC}}$
6Al-4V (STA) titanium forging	RTC	160	Methanol	0.24
	RT	160	Freon M. F.	0.58
	RT	160	N ₂ O ₄ (0.30% NO)	0.74
	RT	160	N ₂ O ₄ (0.60% NO)	0.83
	RT	160	H ₂ O + sodium chromate	0.82
	RT	160	H ₂ O	0.86
	RT	160	Helium, air, or gox	0.90
	RT	160	Aerozine 50	0.82
	90	160	N ₂ O ₄ (0.30% NO)	0.71
	90	160	N ₂ O ₄ (0.60% NO)	0.75
	105	160	Monomethylhydrazine	0.75
110	160	Aerozine 50	0.75	
621-4V titanium weldments (heat- affected zones)	RT	126	Methanol	0.28
	RT	126	Freon M. F.	0.40
	RT	126	H ₂ O	0.83
	RT	126	H ₂ O + sodium chromate	0.82
5Al-25 Sn (ELI) titanium plate	-320	180	LN ₂ (σ < proportional limit)	>0.90
	-320	180	LN ₂ (σ > proportional limit)	0.82
	-423	210	LH ₂	>0.90

TABLE 4. (Concluded)

Material	Temperature ^a (°F)	σ_{ys} ^b (ksi) ^c	Fluid Environment	$\frac{K_{TH}}{K_{IC}}$
2219-T87 aluminum plate	RT	58	Air	0.90d
	-320	66	LN ₂	0.82d
	-423	72	LH ₂	>0.85d
4330 steel 4340 steel	RT	205	Water	0.24
	RT	>200	Saltwater	<0.20
GTA welds: 18 Ni (200) steel 18Ni (250) steel 12Ni-5Cr-3 Mo steel	RT	200	Saltwater spray	>0.70
	RT	235	Saltwater spray	>0.70
	RT	170	Saltwater spray	>0.70
9Ni-4Co-2.5 steel	RT	170	Saltwater spray	>0.70
Inconel 718	RT	165	Gaseous hydrogen at 5000 psig	<0.25

a. $K = (5/9)(°F + 459.67)$.

b. 1 ksi = 6.895 MN/m².

c. Room temperature.

d. No failure K_{TH} , some growth observed at lower values.

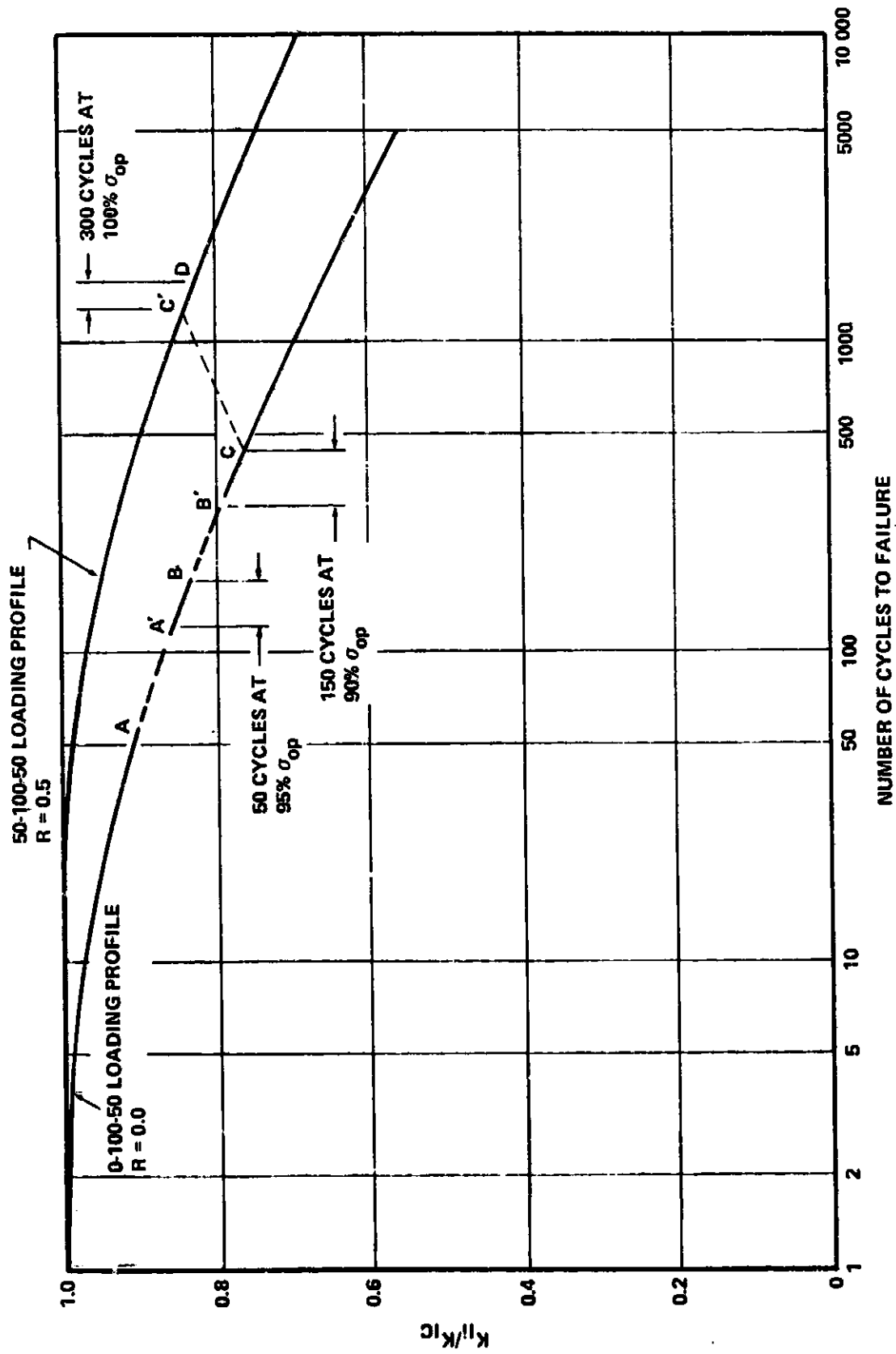


Figure 14. Operating stress levels in a 2219-T87 aluminum tank for a given loading schedule.

With this preliminary information, the design process can now begin. Because of the value of the threshold stress-intensity ratio for sustained crack growth (for this case, 0.90), the allowable value of K_{II}/K_{IC} at the beginning of actual operating cycle at a stress level of σ_{op} is 0.90. This is plainly shown on the lower curve as point A (Fig. 14). Similarly, it is shown as another point A on the schematic representation of the history of cyclic stress loading. Figure 15 is such a schematic representation.

A-A' — Prior to the actual operating cycle at a stress level σ_{op} , there are 50 cycles of stress loading at $0.95 \sigma_{op}$. So, from point A, there will be a decrease of 5 percent from 0.9 or $0.95 (0.90) = 0.855$; i. e.,

$$\left(\frac{K_{II}}{K_{IC}} \right)_{A'} = 0.855 \quad .$$

A' -B — Now measure off 50 cycles from A' to B along the 0-100-0 curve, resulting in

$$\left(\frac{K_{II}}{K_{IC}} \right)_B = 0.83 \quad .$$

B-B' — There is another 5 percent decrease of the stress intensity ratio from 0.95 to $0.90 \sigma_{op}$. This gives a point B' on the same curve corresponding to a stress ratio of $0.95 (0.83) = 0.79$, or

$$\left(\frac{K_{II}}{K_{IC}} \right)_{B'} = 0.79 \quad .$$

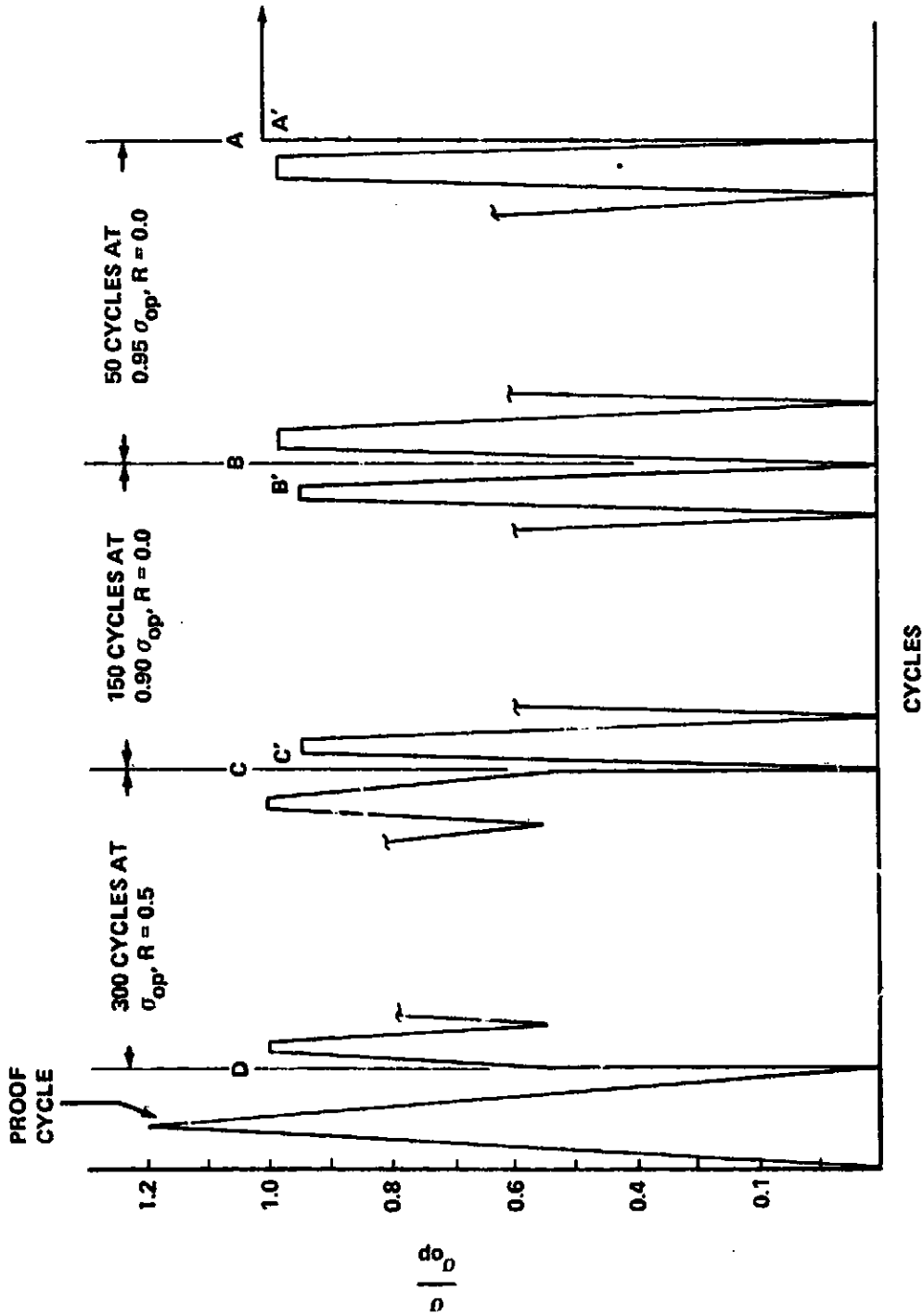


Figure 15. History of cyclic stresses in 2219-T87 aluminum tank.

B' -C - Now measure off 150 cycles from B' to C along the 0-100 curve, arriving at

$$\left(\frac{K_{II}}{K_{IC}}\right)_C = 0.76 \quad .$$

C-C' - The stress loading profile now changes from 0-100-0. (R = 0.0) to 50-100-50 (R = 0.5). This necessitates a change to a new curve - the top curve in Figure 14. Further, the 300 cycles, which scheduled next is at a stress level of 100 percent σ_{op} , a 10 percent increase from that of the previous 150 cycles. The resulting stress level at C' is then $0.76 (1.10) = 0.84$, or

$$\left(\frac{K_{II}}{K_{IC}}\right)_{C'} = 0.84 \quad .$$

C' -D - The 300 cycles at σ_{op} changes the stress intensity from 0.84 to 0.825 which is represented by the point D on the upper curve in Figure 14. Hence,

$$\left(\frac{K_{II}}{K_{IC}}\right)_D = 0.825 \quad .$$

Thus, for the pressure vessel subjected to the scheduled loading history, the maximum allowable stress-intensity factor K_{II}/K_{IC} at the end of the proof cycle is 0.825; that is, the minimum required proof-test factor is $1/K_{II}/K_{IC} = 1.212$. This imposes a restriction on the maximum allowable operating stress σ_{op} (which in this case is $0.825 \sigma_{ys}$) since the proof stress should not exceed the yield stress of the material. Hence,

$$\sigma_{op} = 0.825 \sigma_{ys} \quad .$$

With the allowable operating stress determined as $0.825 \sigma_{ys}$ or $0.825 (70.5) = 58.2$ ksi, the thickness of the tank can be computed from the conventional formula¹ from the hoop membrane stress in cylindrical tanks:

$$t = \frac{PD}{2\sigma_{op}} = \frac{40(400)}{2(58200)} = 0.137 \text{ in.}$$

The critical crack size, which is the greatest crack size that exists in the tank at the proof test stress of $\sigma_{ys} = 70.5$ ksi at -423°F , is

$$\left(\frac{a}{Q}\right)_{\text{allowable}} = \frac{1}{1.21 \pi} \left(\frac{K_{IC}}{\sigma_{ys}}\right)^2 = \frac{1}{1.21 \pi} \left(\frac{32.8}{70.5}\right)^2 = 0.057 \text{ in.}$$

This crack size is significant in that the designer must be assisted by his quality control equipment which can detect crack size smaller than 0.057 in.

Example II

1. Material:

- a. 5 Al-2.5 Sn titanium
- b. Operating temperature, -423°F
- c. Fluid environment, helium
- d. Yield stress, $\sigma_{ys} = 170$ ksi
- e. Ultimate stress, 195 ksi
- f. Critical stress intensity factor, $K_{IC} = 45$ ksi.

1. At this stage of design, an approximate and simple formula is preferred. A refined computation would be in order after a more precise operating schedule for the tank has been established.

2. Loading schedule:

- a. 200 cycles at $0.90 \sigma_{op}$, $R = 0.1$
- b. 4300 cycles at σ_{op} , $R = 0.7$
- c. 260 cycles at $0.5 \sigma_{op}$, $R = 0.4$
- d. 60 cycles at σ_{op} , $R = 0.1$
- e. Long duration flight cycle at σ_{op} .

3. Tank outside diameter 400 in.; maximum operating pressure 40 psig.

Table 4 gives the value of threshold stress intensity for sustained-stress crack growth as $0.90 K_{IC}$, hence, the allowable value of K_{II}/K_{IC} at the beginning of the long flight at σ_{op} is 0.90. This starting point is located at point A on the lower curve in Figure 16. There are three curves in that figure each corresponding to a different value of R. The schematic representation of the history of cycles of stress loading is shown in Figure 17.

A-B — From point A, where

$$\left(\frac{K_{II}}{K_{IC}} \right)_A = 0.90$$

measure off 60 cycles to the right along the curve for $R = 0.1$, arriving at point B (beginning of 60 cycle), where

$$\left(\frac{K_{II}}{K_{IC}} \right)_{B_{R=0.1}} = 0.84$$

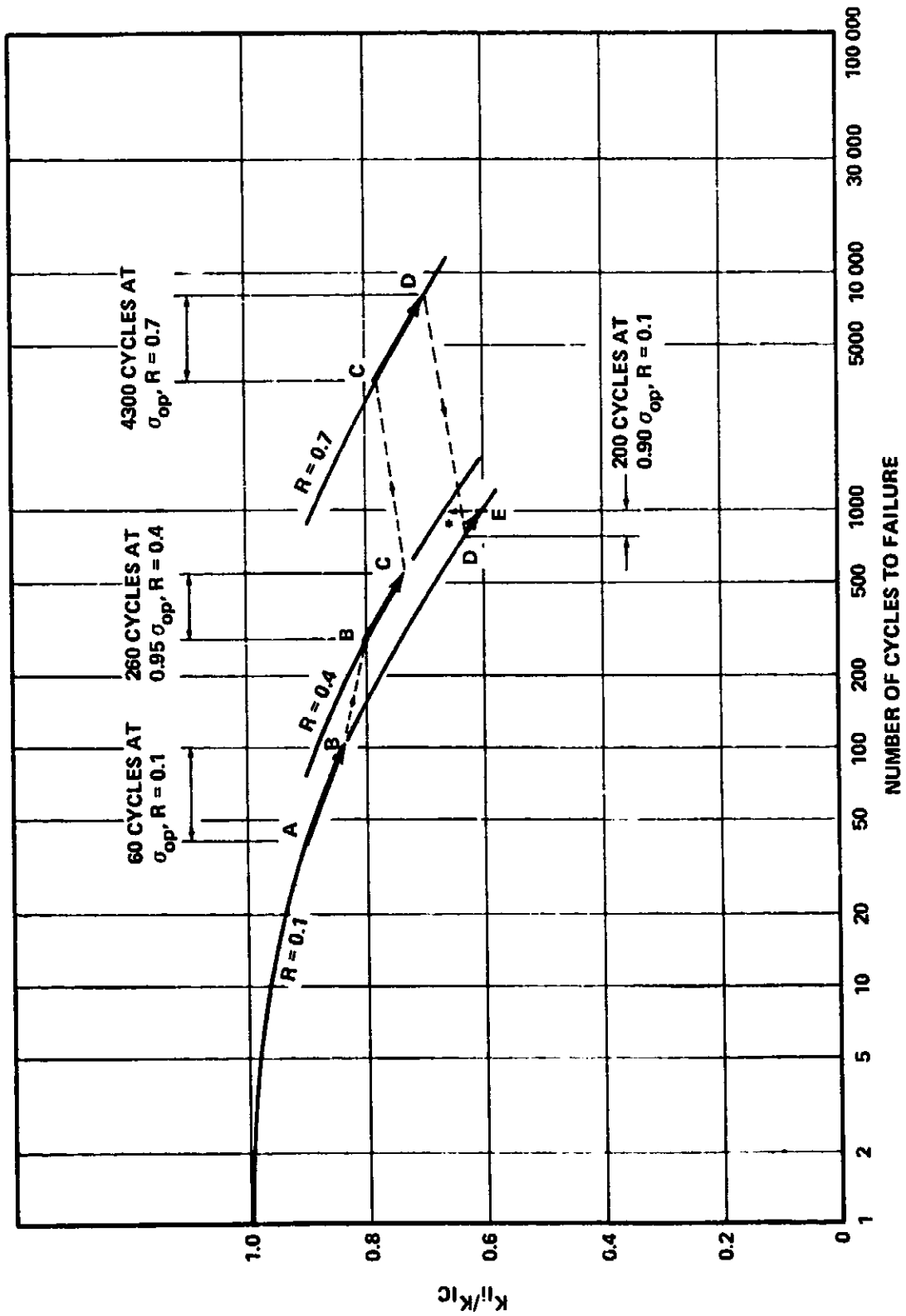


Figure 16. Operating stress levels in a 6 Al-4V titanium tank for a given loading schedule.

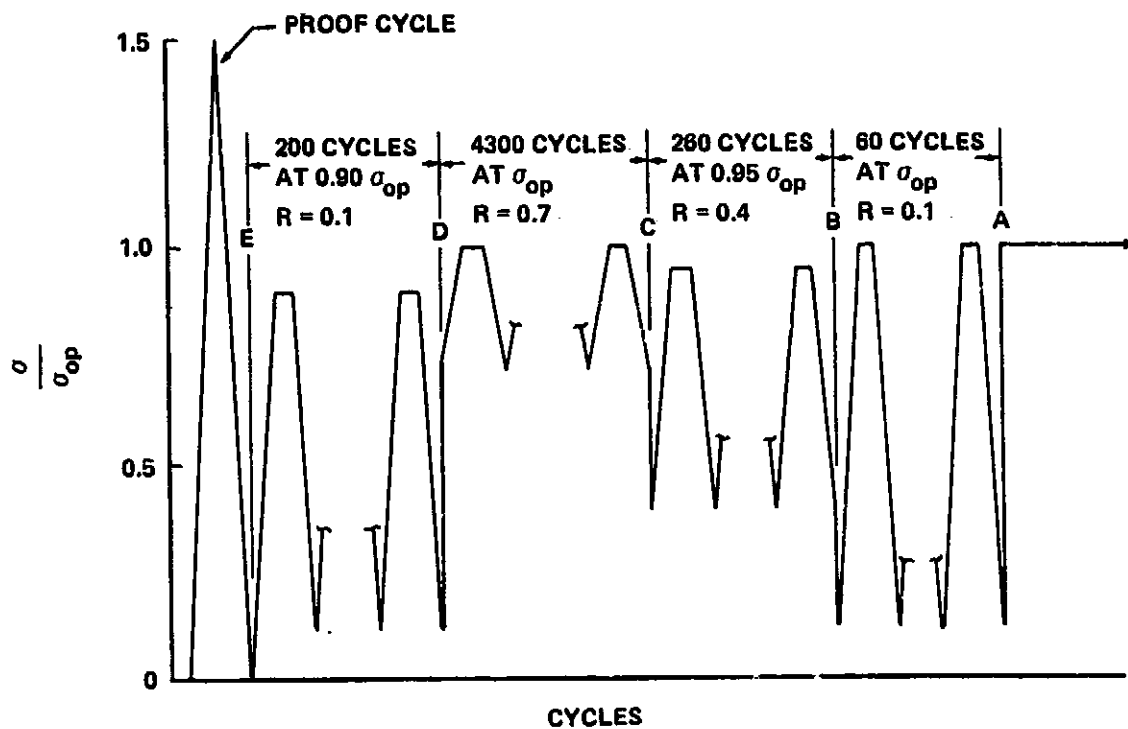


Figure 17. History of cyclic stresses in 6 Al-2.5 Sn titanium tank.

$B_{R=0.1} - B_{R=0.4}$ — There is a decrease of 5 percent of σ_{op} between the points $B_{R=0.1}$ and $B_{R=0.4}$. The latter point is on a curve for $R = 0.4$ and at a value of stress-intensity ratio $0.95 (0.84) = 0.798$, or

$$\left(\frac{K_{II}}{K_{IC}} \right)_{B_{R=0.4}} = 0.798$$

$B_{R=0.4} - C_{R=0.4}$ — Measure off 260 cycles along the curve for $R = 0.4$, arriving at point $C_{R=0.4}$ (beginning of 260 cycles), where

$$\left(\frac{K_{II}}{K_{IC}} \right)_{C_{R=0.4}} = 0.738$$

$C_{R=0.4} - C_{R=0.7}$ - The stress level increases 5 percent from $C_{R=0.7}$; the latter point is located on a curve for $R = 0.7$, where

$$\left(\frac{K_{II}}{K_{IC}} \right)_{C_{R=0.7}} = 0.78 \quad .$$

$C_{R=0.7} - D_{R=0.7}$ - Measure off 4300 cycles at σ_{op} on a curve for $R = 0.7$, arriving at

$$\left(\frac{K_{II}}{K_{IC}} \right)_{D_{R=0.7}} = 0.70 \quad .$$

$D_{R=0.7} - D_{R=0.1}$ - The stress level decreases 10 percent from $D_{R=0.7}$ (at σ_{op}) to $D_{R=0.1}$ (at $0.9 \sigma_{op}$); the latter point is located on a curve for $R = 0.1$, where

$$\left(\frac{K_{II}}{K_{IC}} \right)_{D_{R=0.1}} = 0.9 (0.70) = 0.63 \quad .$$

$D_{R=0.1} - E_{R=0.1}$ - Measure off 200 cycles from $D_{R=0.1}$ along a curve for $R = 0.1$, arriving at

$$\left(\frac{K_{II}}{K_{IC}} \right)_E = 0.6 \quad .$$

At the beginning of the 200 cycles, i.e., E, the stress level is raised 10 percent to σ_{op} ; hence, the actual operating stress is $0.6/0.9 = 0.667$, i.e.,

$$\left(\frac{K_{II}}{K_{IC}} \right)^* = 0.667 \quad .$$

Thus, for the pressure tank under consideration, the maximum allowable stress-intensity factor K_{II}/K_{IC} at the end of the proof cycle is 0.667 and the minimum required proof-test factor is

$$\left(\frac{K_{II}}{K_{IC}} \right) = \frac{1}{0.667} = 1.5 \quad .$$

Hence,

$$\sigma_{op} = 0.667 \sigma_{ys} \quad ;$$

that is,

$$\sigma_{op} = 0.667 (170) = 113.4 \text{ ksi} \quad .$$

With this operating stress the thickness of tank can be computed

$$t = \frac{PD}{2\sigma_{op}} = \frac{40(400)}{2(113.400)} = 0.071 \text{ in.} \quad .$$

The critical crack size at the proof test stress of $\sigma_{ys} = 170$ ksi, is

$$\left(\frac{a}{Q}\right)_{\text{allowable}} = \frac{1}{1.21\pi} \left(\frac{45}{170}\right)^2 = 0.018 \text{ in.}$$

EQUATION (15) AND ITS MEANING

In a previous section, the following equation was derived:

$$\frac{\sigma}{A} \cdot \frac{\Delta N}{\sqrt{a}} = 2 \quad (15)$$

Equation (15) becomes

$$\frac{\sigma}{A} \Delta N = 0.268 \quad (16)$$

for a crack size of $a = 0.018$ in., which was arrived at in Example II for a titanium tank ($K_{IC} = 45$ ksi, $\sigma_{ys} = 170$ ksi). While the constant A is not yet determined, equation (16) can be depicted as a hyperbola: σ/A versus ΔN in Figure 13, where a is a parameter.

Noting that a is dependent only on the material, it is clear that the constant A is primarily dependent on the loading schedule under consideration and through σ on the material. Since in Example II, $\sigma_{op} = 113.4$ ksi at the end of approximately 4820 cycles, one may easily ascertain (at least approximately) the constant A , pertaining to the prescribed loading schedule of Example II, as

$$A = 2.04 \times 10^6 \text{ ksi} \quad (17)$$

Now, equation (16) becomes further simplified:

$$\sigma \Delta N = 5.5 \times 10^5 \text{ ksi} \dots \dots \dots (18)$$

Equation (18) is plotted in Figure 18, a hyperbola relating the operating stress σ_{op} and the number of cycles ΔN for a specific loading schedule for a titanium tank. Equation (18) is valid as long as the loading schedule is not deviated greatly from the given loading schedule, particularly the values of R during the stress cyclings.

Inasmuch as the loading schedule is at most uncertain at this stage of design, equations (16) and (18) may be of use in estimating the safe life of a pressure tank or similar component at different operating stress levels.

DISCUSSIONS

Brittle fractures are characterized by the propagation of cracks at velocities of several thousand feet per second. Most fractures observed are of crystalline texture, indicating that the individual grains of the structural material are fractured by cleavage of crystal planes. In general, there is very little visible evidence of plastic flow. In contrast, ductile fractures show a 45 degree shear tear involving severe plastic deformation of the individual grains. Further, the 45 degree shear fractures develop only by the application of gross plastic overloads approaching the ultimate tensile strength. More importantly, the propagation of such plastic fractures proceeds only at the rates of continued reapplication of the plastic overloads and, therefore, with very high absorption energy. Brittle fractures, however, are propagated in a manner which may be described as "spontaneous" in that the small amount of required driving energy is entirely derived from the release of elastic strain energy.

Brittle fractures may be initiated at conventional design levels of nominal elastic stress, provided certain other conditions are satisfied:

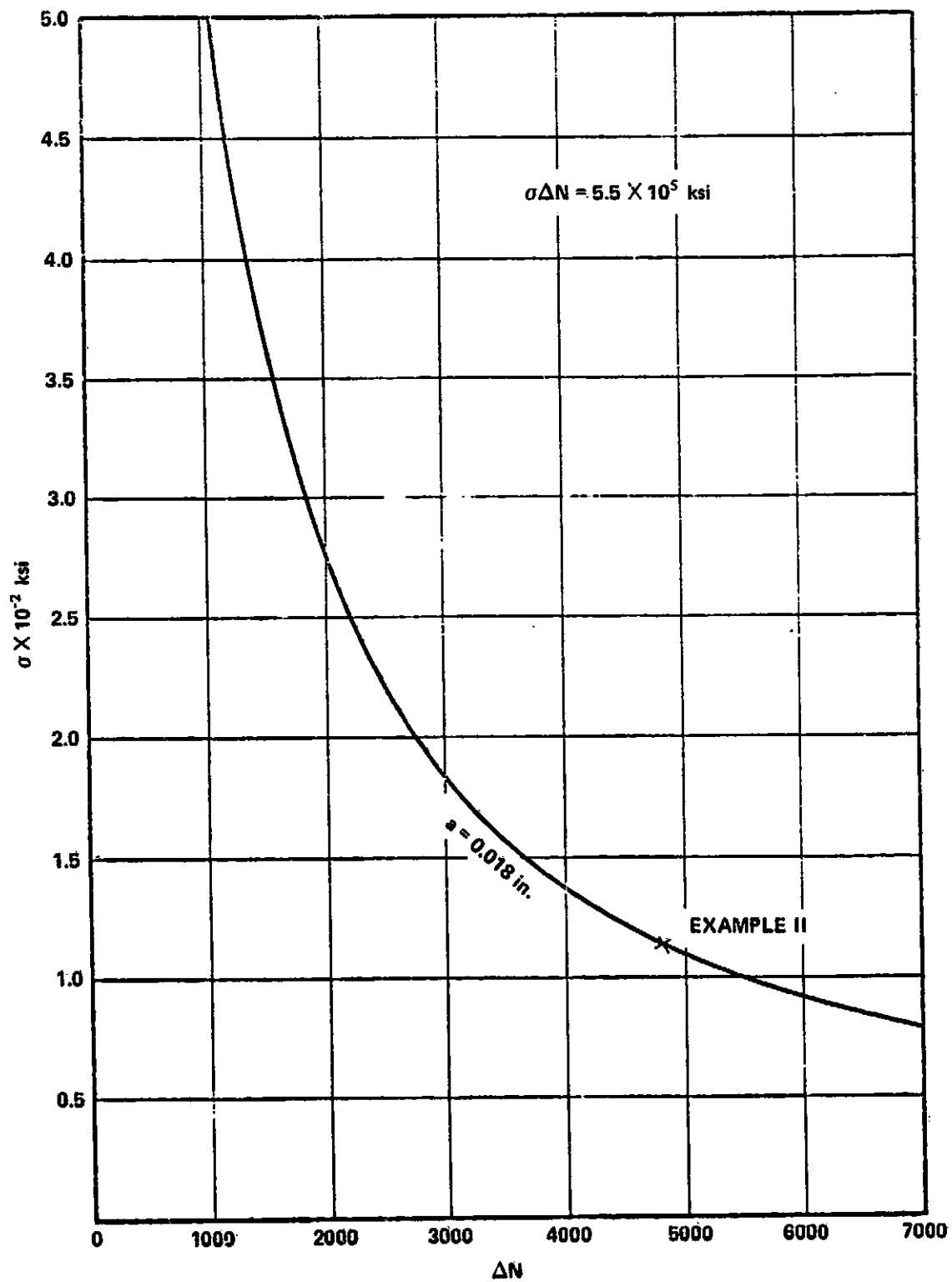


Figure 18. σ versus ΔN Al-2.5 Sn titanium tank for a specific loading schedule.

1. A crack, flaw, or sharp notch is present.
2. The stress is of sufficient intensity to develop a small amount of deformation at the notch tip.
3. The service temperature is low enough to promote cleavage fracture of the deformed metal crystals at the notch tip.

It is clear, then, the initiation of fracture at nominal elastic load level is determined by the cleavage cracking tendencies of a small volume of structural material at the tip of the notch. If plastic deformation occurs there without the presence of a crack, the structure is not endangered because a surrounding larger volume of metal readily assumes the burden of supporting the stress. If cleavage cracking occurs, a sharp natural crack front is extended into the metal by a high-speed repetition of the crack tip cleavage process, resulting in a "propagation" of the brittle fracture.

From the foregoing delineation of brittle fractures as opposed to ductile fractures, it is quite clear the designer would, by all means, have substituted ductile materials for the high strength materials, only if the ductile materials could withstand the high operating stresses and/or at very low operating temperatures. To make the situation even more prohibitive, the designer, hampered already with weight limits on the proposed article or component, is further restricted by limited technology of detecting the smallest cracks, should there be any in the vessel or article.

The second restriction needs explanation. In Example II, if 2219-T87 aluminum had been substituted for the material for the pressure vessel under the identical loading schedule, the results would be:

<u>Material</u>	σ_{ys} (ksi)	K_{IC} (ksi/in.)	$\frac{\sigma_{op}}{\sigma_{ys}}$	σ_{op} (ksi)	$(a/Q)_{CR}$ at Proof Stress (in.)
5 Al-2.5 Sn Titanium	170	45	0.667	113.4	0.018 (see Example I)
2219-T87 Aluminum	70.5	32.8	0.84	59.0	0.057

It is seen that the maximum allowable crack sizes are 0.018 in. in the titanium tank and 0.057 in. in the aluminum tank. This means that any candidate titanium tank with a crack size of 0.018+ in. would be rejected if the designer is capable of detecting such a small flaw size. Difficult as it is to fabricate titanium tanks, it is anticipated that as a result many candidate titanium tanks would be rejected. There will be less number of rejects if aluminum tanks were contemplated for selection because the allowable crack size in aluminum tanks is more than triple that in titanium tanks. However, should the designer or his quality control associates be unaware of their inability to detect a crack size of 0.018 in., a number of accepted titanium tanks could unexpectedly fail during proof test.

Although the titanium tank would be much lighter and superior in every way, it seems ironic that its selection will be weighted against it, simply because nondestructive inspection equipments fail to report such flaws as small as 0.018 in. (a critical flaw size in this particular titanium vessel operating at -423°F).

In view of the foregoing, one may realize that quality control also plays a significant role in the design of high performance components with brittle materials.

Although proof testing guarantees a certain crack size and none greater, sometimes accidental overloading during the service life of the component may cause the crack to grow. Hence, it is hard to predict the actual crack size resulting from the cycling in sustained loadings imposed between the time of initial proof test and the end of the service life.

To alleviate this problem, a new concept in proof testing of reusable space vehicles has recently emerged. Unique and controversial, this concept is called "incremental" proof testing. By definition, incremental proof tests are tests performed at prescribed intervals over the service life of a component. As can be surmised, incremental proof test requirements are established to verify structural integrity of the component or article over only a fractional portion of the service life. It is assumed that the first proof test of the series is performed before the component enters operational service.

Potential advantages of the incremental proof test concept include a reduction in structural weight and an increase in reliability due to the smaller crack growth during service operation that must be taken into account. This approach will also be useful to reverify structural integrity in the event that the

vehicle is accidentally damaged or encounters a more severe operating environment than anticipated in design, or if it is desired to extend the useful life beyond that intended. However, there are often formidable practical problems and limitations (scheduling and cost) associated with the implementation of such a concept. Besides, it seems wasteful to spend a good portion of a component's service life in testing. Naive as it may seem, the uncertainty of structural integrity between service cycles can be, at least in part, alleviated by improved nondestructive inspection. Therefore, it can be said that the prime ingredients of a successful design of high performance, reusable components for spacecraft are (1) accurate information about the candidate materials (σ_{ys} , K_{IC} , at various operating temperatures, etc.), (2) a panoramic knowledge of materials behavior under various loading schedules (for example, curves of K_{II}/K_{IC} versus cycles for various values of R, etc.), and (3) flow or crack detecting capability. The last ingredient is unique in fracture mechanics in that it is independent from and out of control of the designer.

CONCLUSIONS

The studies conducted during this research task have resulted in a simplified analytical procedure which can be utilized to assess the fracture mechanics design requirements of propellant tankage of future large, reusable launch vehicles. A definitive fracture mechanics analysis is dependent upon knowledge of the distribution of stresses within a tank, which is a function of its size, shape, and local discontinuities; specific knowledge of the intended cyclic loading of the tank during its service life; accurate properties data for the candidate structural material in its operating environment; and determination of flaw detection capability for the specific structure in question. Since most of this information is unknown or at best tenuous during the conceptual and preliminary design phases, a simplification of the analytical procedure utilized is justified. The procedure developed is intended for development of parametric data of allowable operating stresses and for comparative evaluation of candidate materials for alternate structural design approaches.

During the second year of this research task, available data for candidate structural materials will be reviewed and curve-fitted for use with the design procedure. The design procedure will be computerized to provide rapid evaluation of alternate design approaches, and the procedure will be applied to specific

--	--	--	--	--	--	--	--	--

launch vehicle concepts under study. Although this design procedure was developed specifically for application to the Heavy Lift Launch Vehicle, it can also be applied to other classes of vehicles which have long service life requirements.

REFERENCES

1. Griffith, A. A.: The Phenomena of Rupture and Flow in Solids. Transaction, Royal Society of London, vol. 221, 1920.
2. Inglis, C. E.: Stresses in a Plate Due to the Presence of Cracks and Sharp Corners. Proceedings, Institute of Naval Architects, vol. 60, 1913.
3. Irwin, G. R.: Analysis of Stresses and Strains near the End of a Crack Transversing a Plate. Transactions, A.S.M.E., Journal of Applied Mechanics, 1957.
4. Sneddon, I. N.: The Distribution of Stress in the Neighborhood of a Crack in an Elastic Solid. Proceedings, Royal Society, London, vol. A-187, 1946.
5. Irwin, G. R.: The Crack Extension Force for a Part Through Crack in a Plate. Transactions, A.S.M.E., Journal of Applied Mechanics, 1962.
6. Paris, P.: Third Annual Workshop in Fracture Mechanics. Chapter VI, Denver, Colorado, 1966.


APPROVAL

THE ROLE OF FRACTURE MECHANICS IN THE DESIGN
OF FUEL TANKS IN SPACE VEHICLES


By Stephen J. Denton and C. K. Liu

The information in this report has been reviewed for security classification. Review of any information concerning Department of Defense or Atomic Energy Commission programs has been made by the MSFC Security Classification Officer. This report, in its entirety, has been determined to be unclassified.

This document has also been reviewed and approved for technical accuracy.



CHARLES R. DARWIN
Director, Preliminary Design Office



JAMES T. MURPHY
Director, Program Development